ELSEVIER

Brachytherapy 5 (2006) 14–26

BRACHYTHERAPY

Robotically assisted prostate brachytherapy with transrectal ultrasound guidance—Phantom experiments•

Gabor Fichtinger[1,*], Everette C. Burdette[2], Attila Tanacs[1], Alexandru Patriciu[1,3], Dumitru Mazilu[4], Louis L. Whitcomb[1,3], Dan Stoianovici[1,4]

[1]*Engineering Research Center, The Johns Hopkins University, Baltimore, MD*
[2]*Acoustic MedSystems, Inc., Urbana-Champaign, IL*
[3]*Department of Mechanical Engineering, The Johns Hopkins University, Baltimore, MD*
[4]*Brady Urological Institute, The Johns Hopkins University, Baltimore, MD*

ABSTRACT

PURPOSE: To report the preliminary experimental results obtained with a robot-assisted transrectal ultrasound (TRUS)–guided prostate brachytherapy system.

METHODS AND MATERIALS: The system consists of a TRUS unit, a spatially coregistered needle insertion robot, and an FDA-approved treatment planning and image-registered implant system. The robot receives each entry/target coordinate pair of the implant plan, inserts a preloaded needle, and then the seeds are deposited. The needles/sources are tracked in TRUS, thus allowing the plan to be updated as the procedure progresses.

RESULTS: The first insertion attempt was recorded for each needle, without adjustment. All clinically relevant locations were reached in a prostate phantom. Nonparallel and parallel needle trajectories were demonstrated. Based on TRUS, the average transverse placement error was 2 mm (worst case 2.5 mm, 80% less than 2 mm), and the average sagittal error was 2.5 mm (worst case 5.0 mm, 70% less than 2.5 mm).

CONCLUSIONS: The concept and technical viability of robot-assisted brachytherapy were demonstrated in phantoms. The kinematically decoupled robotic assistant device is inherently safe. Overall performance was promising, but further optimization is necessary to prove the possibility of improved dosimetry.

Keywords: Prostate; Brachytherapy; Ultrasound; Image guidance; Robotics

Introduction

Transrectal ultrasound (TRUS)–guided brachytherapy is an effective treatment for low-risk prostate cancer (1–3), but still many implants fail or cause adverse side effects. Recent work on intraoperative implant dosimetry has brought most promising results (4, 5), and further improvements are doubtless forthcoming. Intraoperative dosimetry requires precise control and real-time tracking of the implanted needles and sources (6, 7), which assumes precise synchronization between implantation and imaging. Several groups are working on predictive deformable tissue models to compensate for organ motion and deformation during needle insertion (8, 9). An effective use of these models requires the ability to insert needles in arbitrary location and angle and also to include force feedback information. To address the problems noted, we constructed an inherently safe and novel needle guidance robot and integrated this device with a commercial brachytherapy system (Interplant, Computerized Medical Systems, St. Louis, MO). Robotic assistance offers the following multiple potential advantages over the conventional template-based technique: (*1*) consistent and precise needle delivery, (*2*)

Received 29 July 2005; received in revised form 28 October 2005; accepted 31 October 2005.

• In this paper we make extensive reference to the Interplant brachytherapy system manufactured by Computerized Medical Systems (St. Louis, MO). At the time of this research, E. Clif Burdette, PhD, was an employee of the company and before that an employee of Burdette Medical Systems, Inc. No current financial interest exists.

• The robotic devices employed in this research include patented inventions of Stoianovici, Whitcomb, and other JHU personnel, with all rights assigned to The Johns Hopkins University. The patent portfolio has been licensed to Image Guide, Inc., Wilmington, DE, in which Dr. Stoianovici has financial interest.

* Corresponding author. Engineering Research Center, The Johns Hopkins University, New Engineering Bldg, Room B26, 3400 North Charles Street, Baltimore, MD 21218-2682. Tel.: +1-410-516-4057; Mobile: +1-410-562-6955; fax: +1-410-516-5553.

E-mail address: gabor@cs.jhu.edu (G. Fichtinger).

1538-4721/06/$ – see front matter
doi:10.1016/j.brachy.2005.10.003

the ability of positioning the needles in any required trajectory, (*3*) precisely known needle position with respect to the guiding image at all times, (*4*) platform for forthcoming automatic image acquisition and soft tissue deformation compensation, and (*5*) potential reduction of manual handling of seeds and concomitant radiation exposure. A fast and accurate system may also reduce the likelihood and/or severity of edema (10). In the long run, these features may result in the reduction of both systematic and random variability in source placement due to a multiplicity of factors currently related to anatomical variability, technique, training, and experience.

Methods and materials

System design and workflow

The system is schematically depicted in Fig. 1. It consists of three major components: a treatment planning and implant guidance/monitoring computer; a TRUS system including an electronic probe positioning stepper; and a needle placement robot spatially registered to the ultrasound probe. The TRUS probe is secured in an electronic stepper (digitally interfaced to the system computer to register prostate image data), which is mounted on the operating room (OR) table, as used in standard prostate brachytherapy procedures. The anthropomorphic phantom representing the patient is brought into the treatment room, and then the robot is mounted on the table on a bridge structure arching over the abdomen. The robot is spatially registered to the ultrasound images. The real-time ultrasound images are transferred onto a computer that is also situated in the operating room. The relevant anatomy is segmented and reconstructed from the ultrasound images. The preoperative implant plan is imported into the intraoperative model or alternatively, a new implant plan can be created intraoperatively. At this point, the computer has knowledge of the complete implant plan including the ideal entry and target location for each needle.

Next, the coordinates of the first needle are sent to a robot. (Again, the robot is coregistered with the live ultrasound images and the prostate in 3D space.) The robot executes the insertion in four decoupled steps: (*1*) the Cartesian stage moves the needle onto the entry point on the skin, (*2*) the remote center of motion (RCM) stage orients the needle to the target, (*3*) the needle insertion stage inserts the needle into the body and advances it to the predetermined depth, and (*4*) the needle insertion stage retracts the needle and leaves the radioactive seeds in the prostate. The physician supervises each step on the computer screen using transverse and sagittal real-time ultrasound images. To increase safety, the system halts the execution after each step and waits for confirmation from the physician. When the needle is fully inserted but before the radioactive seeds are released, the computer has a nearly accurate knowledge of the location of the needle, with respect to the coordinate frame of the 3D target space. Real-time sagittal and/or transverse ultrasound images are acquired continuously and displayed as the needle is being inserted. An outline of the planned needle position is mapped and superimposed onto the spatially registered prostate images. The computer processes the images and conducts a local search for the needle in the vicinity of its expected position. The physician can apply manual correction before approving the position of the inserted needle.

The computer system updates the dosimetry information based upon the inserted needle position for the physician to examine. If the physician does not agree to the position of the needle, then the needle is pulled out without releasing its payload. When correct needle position is confirmed, the robot retracts the needle and the sources are released. During retraction of the needle, we acquire live ultrasound images. Shadows of the sources appear as they are released from the needle. The computer conducts an initial search in

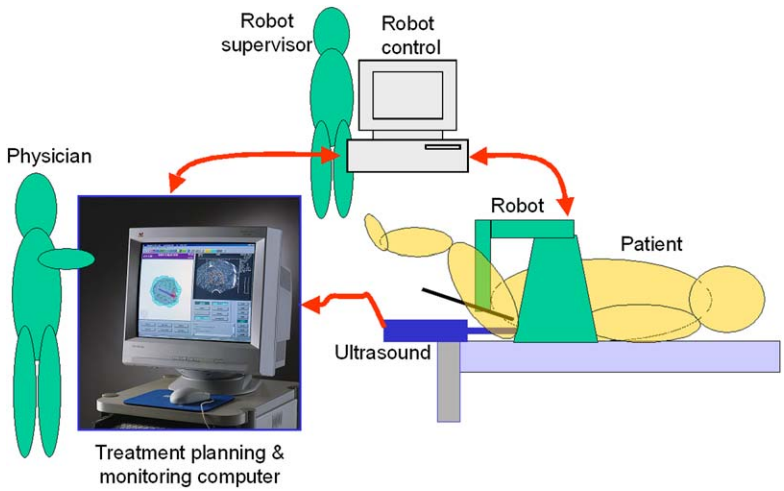

Fig. 1. Systems concept. The system uses a closed digital control loop removing human coordination and measurement errors from the needle placement procedure.

the vicinity of the expected location of the seed. If the computer fails to locate the seeds correctly for reasons like presence of calcifications, then the operator can apply manual correction. Once the seeds are located, the computer promptly calculates full dosimetry, using the sources already implanted in their actual delivered locations, combined with the contribution of the remaining (not yet implanted) planned source locations.

At this point, the physician can modify the remainder of the implant plan, to compensate for deviations from the original dosimetric plan. The cycle of execution is repeated until satisfactory dosimetric coverage is achieved, which is the overall objective of the procedure. The patient is released from the operating room after a satisfactory exit dosimetry is performed. This system uses an image-guided ''point-and-click needle placement'' paradigm, where the physician selects the entry and target points on a computer display of the patient's TRUS-imaged prostate, and a spatially registered robot executes the needle placement under the supervision of the physician. This paradigm can be applied in many other clinical applications as well.

Needle placement robot

Percutaneous needle punctures typically include three decoupled tasks: (*1*) touch down with the needle tip on the skin entry point that requires 3D Cartesian motion, (*2*) orient the needle by pivoting around the skin entry point that requires two independent rotations, and (*3*) finally insert the needle into the body along a straight trajectory that requires 1D translation that may be combined with rotation along the axis of translation (drilling). Several robot systems have been developed for image-guided percutaneous needle placement (11, 12), including embodiments designed or adapted for intraprostatic access. Rovetta (13) performed TRUS-guided biopsy with an industrial robot arm in a telesurgical setting. The authors, in collaboration with others at Johns Hopkins and NIH, demonstrated transrectal robotic biopsy and seed placement in closed high-field MRI scanner (14, 15). Wei *et al.* (16) integrated a commercial serial manipulator with a home-grown 3D TRUS imaging and software platform and evaluated the system in phantoms. Although several promising possibilities were demonstrated, any motion of the needle was accomplished by simultaneous motion of all links controlled by software alone, which is not considered inherently safe. The authors built a two degrees-of-freedom (DOF) RCM mechanism conjunctly with a radiolucent needle driver for percutaneous renal access (17) and used it with C-arm fluoroscopy under joystick control (18) in a system where the stages of translation, fulcrum, and needle insertion were decoupled in an inherently safe manner. This system was further applied in various procedures under computational image guidance with C-arm fluoroscopy (19), CT (20), and CT–fluoroscopy (21). The authors integrated this robot with a stereotactic registration method for transperineal access to the prostate under CT guidance (22) in laboratory experiments. The shortcoming of embodiment, besides using suboptimal CT guidance, was the lack of encoded Cartesian motion.

To address the shortcomings noted, we developed a 6-DOF robot (Fig. 2) that provides fully decoupled 3D translation, 2D rotation, and 1D insertion. The Cartesian motion stage is mounted on a bridge above the patient across the table. Its workspace is 200 mm laterally and 40 mm along the anterior–posterior (AP) and apex–base axes. The spatial resolution is 0.01 mm in each direction. All amplifiers and power supplies are incorporated in the bridge that is connected to the rotational stage by an articulated passive arm providing gross initial positioning. The arm is manufactured from high-quality aluminum alloy, providing structural integrity, stability, and easy machining at reasonably low cost. The rotational stage uses a miniature chain-drive parallelogram structure with one full revolution around each axis with a resolution of 0.01° (18). The needle is inserted and retracted by a linear translational stage using the principle of friction transmission with axial loading (17, 23), with a resolution of 0.01 mm. The insertion stage uses a trapezoid velocity profile with 12.5 mm/s, whereas the maximum velocity of the insertion stage is 25 mm/s. Before insertion, the preloaded needle is secured in the needle driver. After the payload is implanted and the needle retracted, the empty needle is removed from the needle driver and replaced with the next preloaded needle. One separate direct-current motor powers each DOF. The motion stages are fully decoupled and operated sequentially. Only one stage moves at a time while safety switches

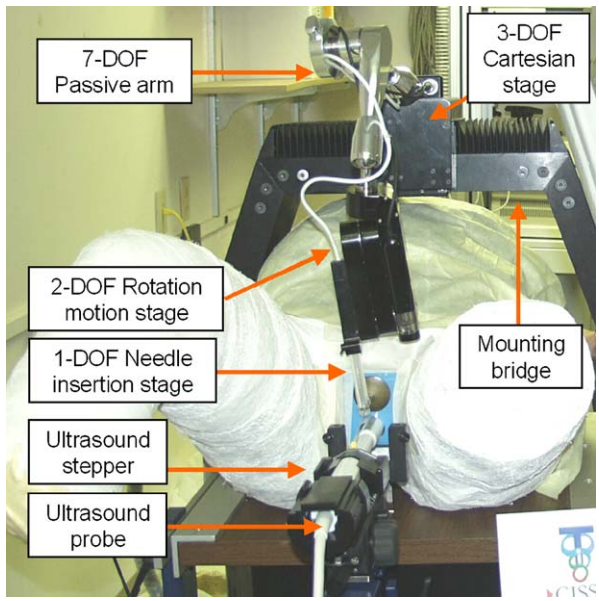

Fig. 2. Close view of the robot. The principal components and motion stages (with indication to their degrees of freedom, or DOF) are labeled individually.

disable all other stages. This scenario prevents insertion before correct alignment is confirmed and also prevents an accidental change in the needle path during insertion. The system also applies a nonbackdrivable transmission that preserves configuration when the robot is deactivated or in the event of power failure. Overtravel of the stages is a concern addressed extensively in the control software and by placing hard-stops on the hardware. Most critically, accidental overtravel of the needle can be prevented by placing a clamp on the needle shaft above the driving gear at the maximum insertion depth. These features provide effective guarantee that the robot performs only the prescribed motion and each component stays within the set constraints. A more detailed engineering description of this robot is available elsewhere (24).

Treatment planning and monitoring software

We used the commercially available Interplant planning and implant monitoring and guidance system, with the addition of specific robotic control software. The Interplant is a Windows-based system that features simultaneous real-time image capture and display from the spatially coregistered ultrasound unit. After the prostate is scanned, the implant plan is created, either intraoperatively or pretreatment. The implant procedure is observed using real-time ultrasound images spatially registered in 3D with respect to the location within the prostate. The system provides semiautomated tools to capture the implanted needle in transverse and sagittal ultrasound images, as the needle is being advanced into the body. When the actual position of a needle is identified, the implant plan is updated. This feature helps the physician achieve optimal dosimetric coverage, even if certain needles were not placed to their ideal locations.

Robot control software

The robot is controlled by the Modular Robot Control (MRC) library, which has been developed at The Johns Hopkins University. The MRC library is a set of portable C++ classes for distributed and modular robot control. The MRC library provides Cartesian-level control for serial manipulators. The control library also includes classes for kinematics, joint level control, command and command table management, sensor and peripheral support, and networking support via remote procedure call. For the benefit of increased safety and modularity, a dedicated computer controls the robot. This computer runs the robot server under Windows NT operating system (Microsoft Corp, Redmond, WA) and is accessed by a client application running on the treatment planning and implant monitoring workstation. The communication takes place via standard Transmission Control Protocol/Internet Protocol connection over a local network. The client application is sealed off from the server and they communicate with the use of a small library of functions, such as *InitializeRobot*, *Move-CartesianStage*, *MoveRotationalStage*, and so forth. Error and exception handling are provided by the robot server. Procedure, error, and status codes are also communicated to the client application, which monitors status and provides any needed alerts to the user.

Quantitative ultrasound guidance

We used commercial TRUS equipment as typically used in prostate brachytherapy. The ultrasound kit included a probe, stepper, table mount, and accessories, all integrated with the complete Interplant system. The ultrasound probe, providing transverse and sagittal images, is secured in a stepper unit. The base of the stepper is mounted on the end of the implant table, and the template is mounted on the stepper's base. A special feature of the Interplant hardware is that the stepper is digitally encoded, so the insertion depth and rotation of the probe with respect to stepper base and template are always known by the central computer and are registered in 3D space with the prostate.

The robot is spatially registered and calibrated to the ultrasound device. We use transrectal ultrasound images for the assessment of needle placement. If the placement is not satisfactory, the supervising physician has two options: (*1*) retract the needle and reinsert it and (*2*) deploy the seeds and recalculate the rest of the implant and thus compensate for potential misplacement of the needle and the effect on delivered dose. If the discrepancy between plan and execution is substantial, the physician may choose reinsertion.

System calibration

The ultrasound stepper and the robot are both rigidly attached to the table, which serves as a rigid mechanical link between the two devices. The approach to setup and calibration was to preserve the FDA-approved features and processes of the Interplant system, without alteration. This was a conscious decision, keeping in mind future clinical as well as commercial deployment. This approach is in sharp contrast to that of Wei *et al.* (16) where a complex precision-machined custom-made calibration phantom was used. In the Interplant system, the TRUS probe is spatially registered to the template, and the stepper is electronically encoded. We opted to register the robot to the template, so the robot became implicitly registered to the TRUS images.

The coordinate frames and transformations implemented in our system are explained in Fig. 3. The target resides in ultrasound image. In the Interplant system, the ultrasound image is calibrated to the template, and the coordinate transformation between the two frames is F_{TU}. Our robot is calibrated to the template, and the coordinate transformation between the two frames is F_{RT}. Any P_U point in ultrasound frame can be addressed in robot frame as P_R, where $P_R = F_{RT} \times F_{TU} \times P_U$. This mathematical formulation will be important later, when we analyze sources of system errors. The template, registered with the probe stepper

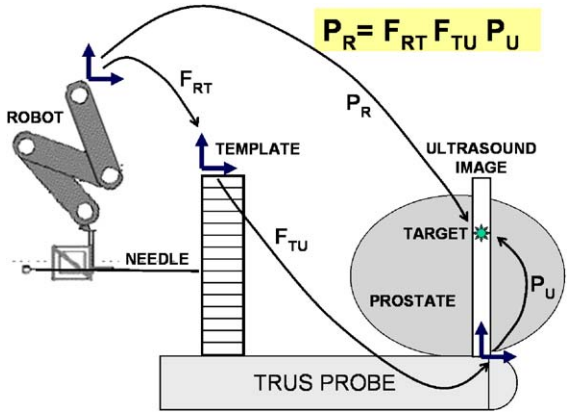

Fig. 3. Coordinate frames and transformations in the robotic system.

provided the common reference frame for the following system components: the Interplant, the ultrasound device, and the robot.

Because the version of the Interplant dose planning module used for this study required that needles be entered perpendicularly to the face of the template, we did not perform calibrated rotational motion with the robot. This also simplified the registration process, which consisted of three simple steps: (*1*) bringing the trajectory of the needle into coincidence with central hole in the lowest template row, and then disabling the rotational motion stage for rest of the procedure; (*2*) aligning the rows and columns of the template with the lateral axis and AP axis of the Cartesian stage, respectively; (*3*) bringing the RCM of the robot to the face of the template. Once these steps are performed, the robot is in home position and coregistered with TRUS space. After the registration took place, we removed the template from the ultrasound stepper.

Experiments and results

Experimental design

We designed several series of experiments with a mechanical phantom to demonstrate the viability of the proposed implementation of the ‘‘point-and-click needle placement’’ paradigm. Three major sessions were performed using mechanical phantoms.

1. *Setup and positioning*: In the first experiment, actual dimensions of human patients were simulated by an anthropomorphic phantom as shown in Fig. 4. A full body plaster cast of one of the investigators was produced (Fig. 4A). We measured aspects of basic

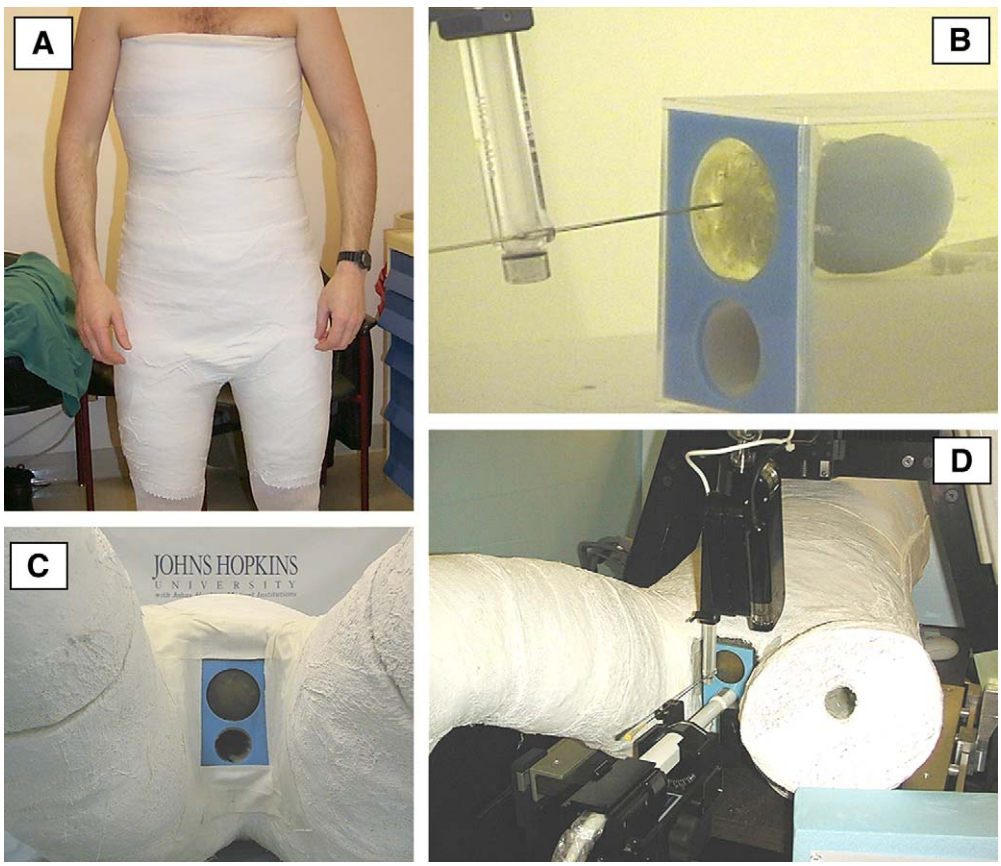

Fig. 4. Anthropomorphic phantom. (A) Full body cast, (B) brachytherapy training phantom, (C) training phantom inserted into the body cast, and (D) fully assembled anthropomorphic phantom in treatment position, with left leg removed.

ergonomics, including ease and safety of patient positioning, robot mounting tolerances, and clearances.
2. *Access and coverage*: A prostate training phantom (Nuclear Associates, Hicksville, NY, Fig. 4B) was inserted into the torso, in a way that the overall size and the layout of organs reasonably represented an average male body (Fig. 4C). The possible locations and angles of needle insertion were constrained by the circular whole on the face of the training phantom.
3. *Needle insertion and tracking*: Finally, a life-size torso with removable extremities was assembled from the cast (Fig. 4D). Our goal was to demonstrate the placement of needles and seeds into mechanical phantoms and seamless integration with the rest of the intraoperative system, especially with real-time ultrasound tracking. We executed the following sequence in the needle placement experiments:

    1. Set up and calibrate the system;
    2. Create an intraoperative implant plan;
    3. Place a needle and seeds into the body with the robot;
    4. Locate the needle and seeds in real-time ultrasound;
    5. Recalculate dosimetry after the needle is inserted;
    6. Repeat from step 3, until done.

Setup and positioning

The patient's body could be conveniently set up under the Cartesian bridge on our standard OR table. The bridge was securely clamped to the existing rails of the table. The RCM robot with the needle driver could be conveniently positioned over the perineum, with good clearance and without collision hazard. The clearance was greater than the maximum range of motion in all motorized DOF. One of the investigators also posed in standard treatment position (i.e. supine in extended lithotomy), without interference with the hardware. This experiment, for safety reasons, was performed in a static setup without powering the robot.

Access and coverage

Six needles were inserted into the anthropomorphic phantom shown in Fig. 4D. An important objective was to achieve upward tilted needle trajectory, which will allow us to avoid interference with the pubic arch in real clinical setting. In this experiment, our primary goal was to prove the ability to place needles in arbitrary tilted direction, within a 25° cone around the apex–base direction. Seeds were not implanted into the prostate. The second objective of this test was to prove that the robot is able to reach all clinically relevant locations inside and around the prostate. These experiments were performed under joystick control. As we mentioned earlier, the rotational motion of the robot was not calibrated in our experiments. Two experimental sessions were conducted with calibrated Cartesian robotic motion and insertion.

Experiments with the anthropomorphic and standard training phantoms proved that the clinically significant volume of the phantom was accessible by the robot. Experiments using an active rotational stage proved the ability to place needles in arbitrary directions, within the specified 25° cone around the base–apex axis, indicating the ability to avoid pubic arch interference in human patients (Fig. 5).

Needle insertion

Needle placement experiments were conducted on a standard commercial prostate implant training phantom. The objective of these tests was to demonstrate the ability of placing needles and seeds at their prescribed locations. The locations were locally referenced to the prostate anatomy and not to a world coordinate system, so the accuracy could be subject to systematic errors in the TRUS imaging. The robot and TRUS were calibrated before each session. Beveled 18 G implant needles (Nuclear Associates, Hicksville, NY) were used. Using the Interplant system, an intraoperative implant plan and dosimetry for the phantom prostate were developed. To facilitate cross checking between the plan and robotic needle placement, the planned needle insertion positions coincided with holes in the conventional template. As discussed earlier, the template provided a reference coordinate frame for the robot, and the template grid was also superimposed on the TRUS images. Thus, we had immediate visual and computational feedbacks to assess whether the robot correctly executed the needle placement with respect to the TRUS image frame.

Six preloaded needles were implanted into the anthropomorphic phantom, as seen in Fig. 4D, and 16 preloaded needles into the solo training phantom as seen in Fig. 4C with the calibrated robot. The accuracy of needle placement

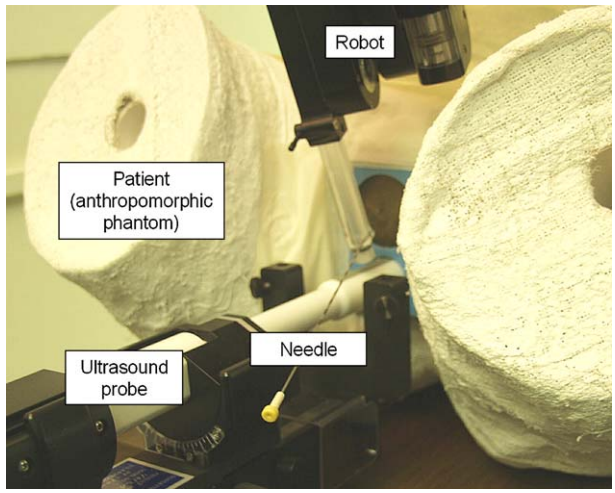

Fig. 5. Upward needle trajectory demonstrated in anthropomorphic phantom. The needle is tilted with respect to the ultrasound probe, in an angle sufficient to avoid pubic arch interface.

was measured in real-time transverse and sagittal ultrasound images, which were spatially registered with respect to each other and to the prostate. The uncertainty in identifying the location of a needle in ultrasound was not specifically determined for this experiment. The center of the needle image was used for the centerline of the needle. As summarized in Table 1, the average aiming error measured in the transverse plane was on the order of 2.0 mm; the worst case was 2.5 mm, and 80% of the insertions landed within a 2 mm transverse margin. The average depth error measured in the sagittal plane was in the order of 2.5 mm, the single worst case was 5.0 mm, and 70% of the needles landed within a 2.5 mm depth margin. It is important to note that these errors include needle deflection in the tissue phantom. These accuracies were achieved without adjustment of the needle.

Ultrasound-based tracking

Fig. 6 shows a screen capture of the Interplant system during needle insertion with a transverse ultrasound image. The screen contained a real-time transverse ultrasound image taken in the intended depth plane of the needle tip. The boxes indicate ideal planned needle positions coinciding with template grid points. The circle shows the actual position of the needle, as seen in the ultrasound image. The circle was drawn by the image processing software around the needle tip location, which is in visually good coincidence with planned needle location. Fig. 7 shows a screen capture of the Interplant system during needle insertion with a sagittal ultrasound image. A sequence of hollow boxes marks the intended position of the needle. The white image track created by the needle indicates the actual position of the needle, which is in visually good coincidence with its intended location. Fig. 8 shows a screen capture of the Interplant system with a sagittal ultrasound image acquired as the needle was retracted, and the exposed seeds were left behind in the phantom. The Interplant located the seeds in the sagittal ultrasound view and updated the dosimetry computation; recalculated isodose lines can be seen around the seeds.

Discussion

Considering a highly experimental prototype and the implicit calibration between the robot and ultrasound, the results that we obtained were promising, although not as impressive as an expert clinician can produce with conventional template technique. It must be noted that in our experiments the needles were not adjusted after insertion. This is in contrast to actual practice, where the clinician adjusts and/or sometimes fully reinserts the needle until satisfactory placement is determined in the real-time ultrasound image. Again, this was not the case in our experiments, where we recorded the result of the first insertion attempt for each needle.

Table 1
Placement error of 22 needles measured in transverse and sagittal images

	Average (mm)	Worst case (mm)	Error distribution
Transverse error	2.0	2.5	80% in 2.0 mm margin
Sagittal error	2.5	5.0	70% in 2.5 mm margin

We must also reemphasize that the long-term significance of robotic assistance is consistency and the ability to synchronize ultrasound imaging and seed/needle tracking. These feasibility experiments did not allow for drawing a strong statistical conclusion. We decided not to amass more trials with this particular system embodiment, because existing calibration errors would not allow for significant reduction in accuracy, and relatively high standard deviation would have remained in the results. In ongoing further work, we have turned our attention to reimplementing the robot hardware and calibration process, as we outline later in this section.

The 2.5 mm average placement error measured in the phantom experiments can be attributed to several main sources as follows: calibration, imperfect position measurement in ultrasound, needle deflection, and tissue stress/deformation. Issues that are specific to robotic assistance must also be considered.

Calibration

As depicted in Fig. 3, our robot was registered to the conventional template and then through the template to the TRUS images, implicitly. Freehand template-based systems are known to have approximately 1.0 mm accuracy in water phantoms. This is a residual system error in ultrasound-to-template transformation after calibrating the commercial FDA-approved Interplant, i.e. this error cannot be removed from our system.

To analyze the registration error between robot and template, we picked several holes on the template and tested whether the robot was able to target the holes on the template. The system was successful in completing these tasks, meaning that the error introduced by the robot system was in the order of half the size of the template hole, about 1 mm. Much of this error is associated with the calibration between the robot and template coordinate systems, because errors from the robot hardware are negligible compared to registration and calibration errors (18, 24). Note that the robot-to-template calibration was accurate on the face of the template, but the insertion depth magnified the error in the target plane.

An effective way to reduce robot-to-TRUS calibration error would be to mount the robot mechanically on the TRUS stepper and calibrate the robot directly to the TRUS image. This, however, requires a small and light custom-made robot, the concept of which we describe later in this section.

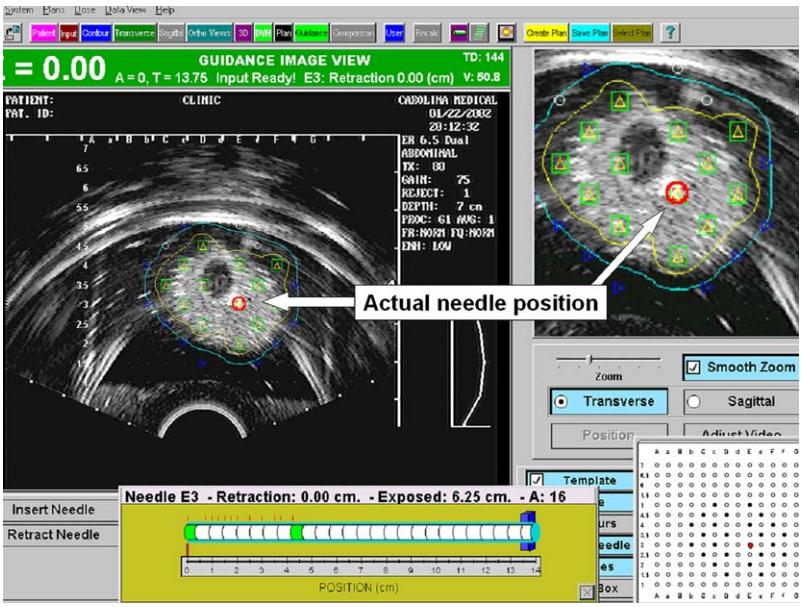

Fig. 6. Transverse view during needle insertion. Square boxes mark the planned needle positions. The circle marks location of the needle tip showing the actual needle position, as it was seen in the real-time transverse ultrasound image. The isodose lines were updated, assuming that the seeds would be released in their ideal relative positions with respect to the needle.

Ultrasound feedback

The accuracy of needle insertion was measured in real-time transverse and sagittal TRUS. The position of the needle tip in TRUS was compared to the implant plan. The accuracy of measurement thereby was limited by the fidelity of the ultrasound, which (due to speckle and inherent systemic errors) typically does not allow for highly accurate readout of the location of needles and seeds. The precision and reliability of ultrasound-based needle and seed detection were not analyzed in this experiment. We captured the location of the needle in TRUS and recalculated the dosimetry, but we did not optimize the plan intraoperatively and did not evaluate the final dosimetric coverage, because the end points of these trials were to evaluate the feasibility of the robotic assistant and overall workflow.

Although we observed the needle in real-time ultrasound, we did not apply this information to dynamically adjust the trajectory of the needle. As we discussed earlier,

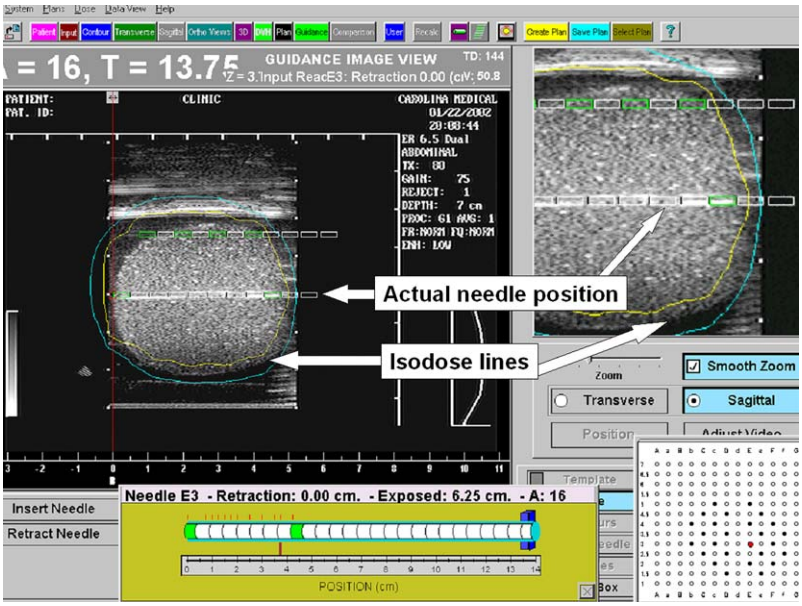

Fig. 7. Sagittal view during needle insertion. Line of boxes marks the intended positions of needle. White needle track shows its actual location, as it was seen in the real-time sagittal ultrasound image. The isodose lines were updated, assuming that the seeds would be released in their ideal relative positions with respect to the needle.

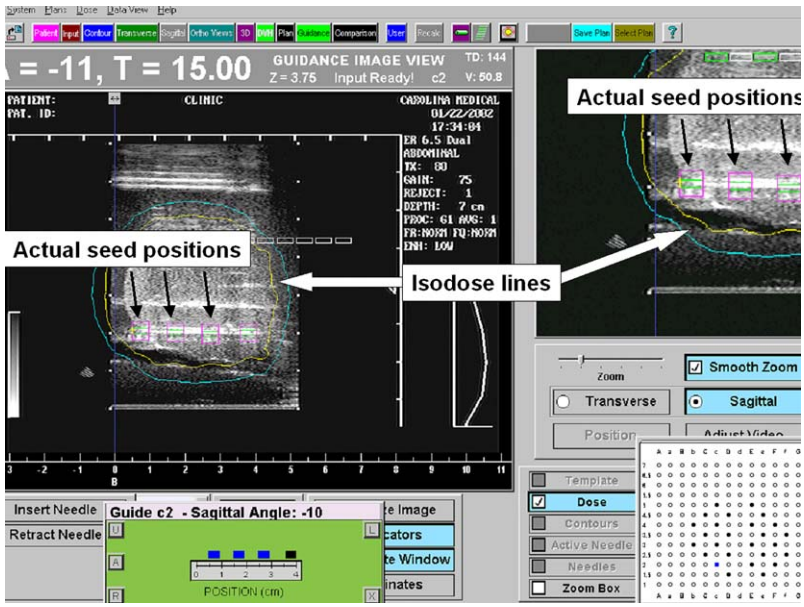

Fig. 8. Sagittal view during needle retraction. Disjoint square boxes mark the actual position of seeds because they were identified in the real-time sagittal ultrasound image by the image processing software after the needle was fully retracted, and then the isodose lines were updated.

computational tracking of the target and actual needle positions in real-time ultrasound is a potentially powerful tool that is expected to lead to manifold improvements in intraoperative dosimetric optimization. Upon withdrawal of the needle, the prostate often responds with a complex motion and deformation despite the presence of stabilizing devices. This causes the final position of seeds with respect to relaxed prostate anatomy to be different from the position determined upon releasing the seeds from the needle. Nevertheless, the search area is sufficiently confined, so that one can track the seeds in the relaxed prostate after the needle is completely removed. This function, however, requires more advanced ultrasound image processing functions currently under development in our laboratory, including tissue deformation models. It is also worth noting that an arbitrary slanted needle trajectory generally cannot be captured in a single US plane. Therefore, future motorization and electronic control of the TRUS stepper seem to be highly desirable, similar to ongoing work of Wei *et al.* (16). They, however, use only sagittal TRUS images that the overwhelming majority of practitioners do not prefer. At the same time, in the more generally preferred transverse imaging, the probe is pressed against the prostate, deforming and/or displacing when the probe translates between the axial planes, which introduces another error. The prudent approach therefore seems to be using both sagittal and axial imaging, and swapping between the two modes as the operating physician finds it appropriate. Most modern TRUS probes provide electronic switch over between the sagittal and axial imaging modes.

It must be mentioned that a significant shortcoming of TRUS is its inability to recover all implanted seeds, which is a prerequisite for intraoperative real-time dosimetry (4–7). Current ultrasound segmentation technology can recover only about 70% of the implanted seeds. The greatest sources of hidden seeds are acoustic shadowing (seeds proximal to the TRUS probe block the signal) and signal deflection caused by perturbation of the seed axis with respect to the needle path. However, confining the search to a small region during and immediately after retracting a needle may yield improved seed localization accuracy. Using high-end ultrasound does not seem to solve the problem of clinically sufficient seed recovery. Therefore, auxiliary information, such as coregistered C-arm fluoroscopy, may be necessary. Ongoing work in this direction by Zelefsky *et al.* has produced promising preliminary results (4, 5).

Needle deflection

Ideally, the needle should be perpendicular to the skin surface to avoid slippage and minimize deflection of the needle during penetration. Inhomogeneity in the transperineal and prostatic tissues causes additional errors. The training phantom was reasonably homogeneous, so the distribution of error could be considered homogeneous throughout the entire prostate, unlike in human patients, where placement accuracy in apex, base, and midgland is expected to vary. Nevertheless, the phantom prostate became slightly deformed, and the needle suffered some deflection.

Needle deflection could be reduced by using thick walled needles (of the type available from World Wide Medical Technologies, Woodbury, CT) or un-beveled needles. Spinning the needle while advancing it could reduce friction and tissue resistance, thereby also reducing the deflection of the needle. Our next-generation needle driver design (25), in

which rotation and translational insertion can be arbitrarily combined, promises major reduction in needle deflection. This can be conjectured from parallel work by Wan *et al.* (26), where needle and seed placement accuracy were significantly improved with bidirectional needle rotation.

In relation to needle deflection, it must be said that in ultrasound-guided needle placement systems it is exceedingly difficult to assess purely technical/engineering accuracy, i.e. to measure the combined hardware, calibration, and image-based targeting accuracy while excluding needle–subject interaction. The ideal solution would be to submerge cross wire target phantoms in a water tank, as customary in the calibration of tracked ultrasound systems (27). In our case, however, the TRUS probe is horizontal, which precludes the use of a water tank. Therefore, we were confined to using a solid gel phantom that unavoidably caused some amount of deflection of the beveled implant needles.

Organ motion and tissue deformation

Prior and current experiments with the needle placement robot suggest that the primary cause of needle placement error, besides calibration, is needle–tissue interaction. Motion of the prostate specimen during needle insertion was not a prominent problem in the phantom experiments, but this phenomenon in human patients must be carefully considered. The penetrating implant needle usually induces deformation and displacement of the prostate gland. Depending upon the mechanical characteristics of the prostate and prostate capsule, this could present a significant problem in the human body. Some practitioners prefer mitigating organ displacement by bilateral invasive fixation with transperineal locking needles (28). This approach, however, has not gained popularity, probably because the extra needles increase tissue damage and the risk of edema. It also seems that correlation exists between needle trauma and acute urethral toxicity (29), discouraging the use of invasive target fixation.

Spinning the needle while advancing it could reduce tissue resistance, thereby also reducing deformation and displacement of the prostate. The aforementioned prototype of the spinning needle driver (25) could be a valuable tool in solving this problem. The transrectal ultrasound probe reduces the effects of peristaltic movement of the rectum, and respiration is not a significant factor.

The effect of eventual motion of the target is mitigated by the real-time imaging system and fast control of the robot. After the target is identified in the live ultrasound image, the robot can start moving onto this target without noticeable delay, reducing the probability of displacement of the target. Once the needle is inserted into the body, the trajectory cannot be changed. However, a maximum acceptable error in needle position can be set in the Interplant system, which can provide a feedback control signal to the robot. The physician/operator can decide whether to have the robot retract the needle to near the skin surface and reinsert the needle into the prostate.

For completeness, we also mention the ongoing research by Rohling *et al.* (30) on motorized needle driver where needle trajectory can be modified while the needle is being inserted.

Needle positioning

The mechanical components of the system were tested under controlled laboratory experiments at the time of constructing the robot. With the needle insertion stage alone we experienced a systematic needle placement error of 0.5 mm in open air, where there was no interaction with target tissue. This error originated from the fact that the needle was slightly incorrectly inserted into the needle driver. The combined errors of the Cartesian bridge and the RCM stage were in the order of 0.05 mm (18, 24).

The robot hardware presented in this paper successfully demonstrated the concept of decoupled Cartesian and RCM stages in prostate brachytherapy use. The design of such structures is inherently safe, because the motion stages in all DOF are sequentially activated, and their range of motion is constrained (18). By conscious design, decoupled robots cannot run in arbitrary trajectory, and it is precisely this constraint that makes them inherently safe. This is in contrast to the industrial serial robot used by Wei *et al.* (16) that is controlled and constrained by software alone, hence it must be considered less safe.

The robot we used, however, was not particularly optimized for prostate brachytherapy. It was rather large and heavy to handle. Although it did not intrude the field of action over the perineum, the Cartesian bridge prevented the use of C-arm fluoroscopy over the abdomen, which is a major impediment that must be eliminated before the system is considered for clinical use.

We will address these issues in the next generation of the robotic assistant, currently under development. This device will be much lighter and smaller than the current robot seen earlier in Fig. 2. The ideal solution seems to be a custom-made minirobot, such as the one envisioned in Fig. 9. Here, a small and lightweight ‘‘parallel robot’’ docks into the place of the template on the base of the TRUS stepper. The particular kinematic details of parallel robots are not relevant for this discussion, and we refer the reader to prior studies with a similar needle placement robot (31, 32). This new parallel architecture robot is conceptually identical to the present system, in that it also provides decoupled constrained Cartesian, fulcrum, and needle insertion motions.

The new robot will reside above the TRUS stepper where it does not block the view to the perineum, and also leaves clear access to lower abdomen, where the C-arm is usually placed. The robot will be mounted directly on the base of the TRUS stepper in a repeatable manner, thus it will be calibrated only once during assembly and certification. The need for preoperative calibration is a major impediment

in our current system, just as it was the case in the systems of Rovetta *et al.* (13) and Wei *et al.* (16). Note that, although the template will not be present in the new robot system, the calibrated mounting posts on the stepper base should be retained for mounting the robot. This is in keeping with our principle of system modularity and preserving the integrity of the previously FDA-approved Interplant system. These requirements exclude all existing industrial robots, such as the ones previously used by Rovetta *et al.* and Wei *et al.* (13, 16).

The preliminary design of the new robot in Fig. 9 promises significant reduction in calibration error by calibrating the robot to the TRUS image directly, with the use of the existing calibration currently available in the Interplant system. The confines of this paper preclude a detailed description of the calibration toolkit, and we only outline the process briefly. Upon mounting the template on the base of the TRUS stepper, the stepper (with the TRUS probe and template on it) is detached from the mount. The tip of the TRUS probe is merged in a water tank. Several needles are inserted through the template into the water bath. The needle tips are located in template space and ultrasound space. Finally, the calibration is completed by calculating the rigid body transformation matrix between the two sets of needle tip locations. In the calibration of the new robot system (Fig. 9) the small and lightweight robot replaces the template, thus the system can be calibrated with the existing same toolkit, without modification. Now the absolute geometrical accuracy of the new system, without needle deflection caused by needle–subject interaction, will be measured in the water tank used for system calibration. The new robot system will be calibrated only once during system assembly and installation. There will be no need for preoperative calibration before every procedure, thereby significantly improving on our current system and other existing works (13, 16). At the same time, we will fully preserve the integrity of the FDA-approved Interplant system.

Needle driving

The current needle driver mechanism uses a friction transmission, which limits the maximum insertion force. If the resistance of the tissue is greater than the maximum transmission force, then the needle will slip axially and stop short of the target. We experienced occasional slippage of the needle in the experimental studies. But as we follow the needle in real-time ultrasound, it can always be inserted deeper on the basis of visual feedback, until the correct depth is reached. Another shortcoming of the current needle driver is that it cannot release its grasp on the needle while the needle is inside the body. This is an important safety issue, if involuntary movement of the patient can be anticipated. We intend to address this problem in an improved second-generation needle gripper implemented in a new needle driver design (25).

We also consider the alternative of manual needle driving augmented with an optoelectronic depth encoder currently under development in our laboratory. The net benefit from this scenario is that the surgeon retains full control and sensation of the needle action, while enjoying full digital integration. This solution would ultimately decouple the surgical intervention from targeting and planning, which is the safest possible proposition. On the end-effector of the robot, a tubular needle guide would keep the needle in the selected trajectory, similarly to the guide holes on contemporary templates. The travel of the needle through the needle guide is measured by an optical encoder array that is able to track the circumferential fiducial stripes on brachytherapy needles with submillimeter resolution.

Seed migration

In the human body, the major source of discrepancy between desired and actual seed positions occurs after the seed is released from the needle tip. Unfortunately, this phenomenon could not effectively be simulated in phantoms, but prior experience with the problem provides some insight. When the seeds are released, the prostate tissue is usually mechanically stressed. When the needle is retracted, the tissue relaxes and the loose seeds drift with it. Furthermore, the retracting needle may cause some suction effect that tends to pull the seeds back along the needle tract. Previously mentioned work by Wan *et al.* (26)

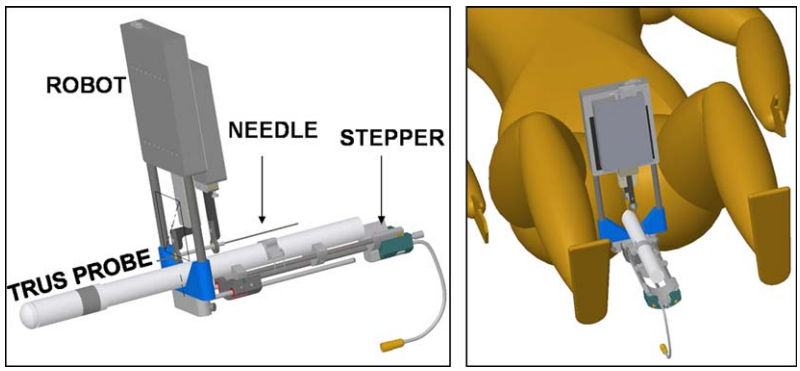

Fig. 9. Design of a parallel minirobot mounted on the template posts on the base of the Interplant. TRUS stepper (left). The robot will be situated over the abdomen during the procedure (right).

indicated that seed placement accuracy can be improved by bidirectional needle rotation during insertion and seed release. In our experience, relatively slow speed of retraction and providing stability for the plunger/trocar during retraction seem to be important mitigating factors. Good initial setup (i.e. applying the optimal rectal pressure with the probe) can also assist in reducing the buildup of mechanical stress on the prostate. For completeness, we mention the alternative of using stranded seeds. This approach, however, has been debated and not preferred by many clinicians.

Setup, positioning, and coverage

The phantom experiments demonstrated easy setup and positioning. There was no collision between the hardware and the subject. We achieved adequate working volume and dexterity. All clinically significant locations in the prostate gland were adequately covered from all relevant access angles. It must be noted, however, that the 40 mm working range of the Cartesian motion stage in the AP direction barely covered the prostate gland in the training phantom. We suspect that this length of travel will not be sufficient in human patients or it would cause significant difficulties in setting up the patient for treatment. A working perineal area of 60×60 mm is planned for the next-generation robot.

Conclusions

We have developed a robotic system capable of delivering needle patterns across the perineum into the prostate, guided by real-time transrectal ultrasound spatially registered with the robot. In the controlling systems software, we implemented intraoperative semiautomated detection of needles and seeds, as they are being deployed in the prostate. Once the needle and seed locations are captured, the dosimetry of the implant is updated. These novel features are integrated with a commercially available prostate brachytherapy planning and monitoring system.

We have demonstrated the concept and technical feasibility of the robotic assisted implant system. Experiments with mechanical and anthropomorphic phantoms indicate that this robotic system may be suitable for transperineal prostate brachytherapy and possibly for a variety of other clinical applications, inside the prostate as well as in other anatomical targets. Major redesign of the robot hardware and needle/seed tracking modules is in progress. Significant further efforts are needed to evaluate the accuracy, safety, and added benefits of the robotic assistant. Initial experiences, however, have been encouraging toward these goals.

In our vision, the role of medical robotics is not process automation, but providing optimal coupling among digital information (i.e. ultrasound imaging), physical action (i.e. seed deposition), and procedural outcome (i.e. dosimetry). The long-term significance of robotic assistance is increasing the consistency of performance toward achieving the optimal dosimetry plan. This is best achieved by providing computer-controlled synchronization among ultrasound imaging, needle insertion, seed deposition, and dosimetry update. In the implantation of a hundred-or-so radioactive seeds, the most important question is not whether any one particular seed can be implanted with pinpoint accuracy, but whether clinically significant accumulation of dosimetric error can be prevented by frequent update of the plan. Although accuracy is very important, the overall goal is optimal dose. This trend is clearly underlined by recent work on intraoperative dosimetry optimization, for example, by Zelefsky *et al.* (4). We firmly believe that robotic assistance, properly synchronized with real-time imaging, can assist in reaching that ultimate goal of optimal dosimetry coverage. This paper does not attempt to solve this extremely complex problem in its entirety. Our work represents one step forward by introducing the concept and initial prototype of a robotic assistant. This device, by conscious design decisions, is inherently safe and may have a role in assisting prostate brachytherapy. The next phase of our efforts will concentrate on optimizing the design of the robotic assistant and its integration with the spatially registered real-time ultrasound imaging and dosimetry computation modules.

Acknowledgments

We gratefully acknowledge the longstanding support of Louis R. Kavoussi, MD (Brady Urological Institute) and Theodore L. DeWeese, MD (Department of Radiation Oncology). We are obliged to Kevin Cleary, PhD, of the Georgetown University ISIS Center, for graciously lending robotic hardware for our experiments. We thank Anton Deguet, MS and Herve Mathieu, PhD for spending endless evening hours with us on the validation experiments. We are grateful to Gernot Kronreif, PhD (Austrian Research Laboratories) for providing the robot design pictures (Fig. 9).

Funding was made available by the National Cancer Institute under 5R44CA088139-04 and by the National Science Foundation under EEC #9731478.

References

[1] Zelefsky MJ, Hollister T, Raben A, *et al*. Five-year biochemical outcome and toxicity with transperineal CT-planned permanent I-125 prostate implantation for patients with localized prostate cancer. *Int J Radiat Oncol Biol Phys* 2000;47:1261–1266.

[2] Merrick GS, Butler WM, Lief JH, *et al*. Is brachytherapy comparable with radical prostatectomy and external-beam radiation for clinically localized prostate cancer? *Tech Urol* 2001;7:12–19.

[3] Blasko JC, Mate T, Sylvester JE, *et al*. Brachytherapy for carcinoma of the prostate: Techniques, patient selection, and clinical outcomes. *Semin Radiat Oncol* 2002;12:81–94.

[4] Zelefsky MJ, Yamada Y, Marion C, *et al*. Improved conformality and decreased toxicity with intraoperative computer-optimized

transperineal ultrasound-guided prostate brachytherapy. *Int J Radiat Oncol Biol Phys* 2003;55:956–963.

[5] Todor DA, Zaider M, Cohen GN, *et al*. Intraoperative dynamic dosimetry for prostate implants. *Phys Med Biol* 2003;48:1153–1171.

[6] Yu Y, Anderson LL, Li Z. Permanent prostate seed implant brachytherapy: Report of the American Association of Physicists in medicine task group no. 64. *Med Phys* 1999;26:2054–2076.

[7] Nag S, Ciezki JP, Cormack R, *et al*. Intraoperative planning and evaluation of permanent prostate brachytherapy: Report of the American Brachytherapy Society. *Int J Radiat Oncol Biol Phys* 2001;51:1420–1430.

[8] Alterovitz R, Pouliot J, Taschereau R, *et al*. Needle insertion and radioactive seed implantation in human tissues: Simulation and sensitivity analysis. Proceedings of the IEEE International Conference on Robotics and Automation; 2003.

[9] Shen D, Lao Z, Zeng J, *et al*. Optimization of biopsy strategy by a statistical atlas of prostate cancer distribution. *Med Image Anal* 2004; 8:139–150.

[10] Yamada Y, Potters L, Zaider M, *et al*. Impact of intraoperative edema during transperineal permanent prostate brachytherapy on computer-optimized and preimplant planning techniques. *Am J Clin Oncol* 2003;26:e130–e135.

[11] Cleary K, Nguyen C. State of the art in surgical robotics: Clinical applications and technology challenges. *Comput Aided Surg* 2001;6: 312–328.

[12] Taylor RH, Stoianovici D. A survey of medical robotics in computer-integrated surgery. *IEEE Trans Rob Autom* 2003;19:765–781.

[13] Rovetta A. Tests on reliability of a prostate biopsy telerobotic system. *Stud Health Technol Inform* 1999;62:302–307.

[14] Fichtinger G, Krieger A, Susil RC, *et al*. Transrectal prostate biopsy inside closed MRI scanner with remote actuation, under real-time image guidance. In: *Proceedings to Medical Image Computing and Computer-Assisted Interventions 2002*. *Lecture Notes in Computer Science*, Vol. 2488. Springer-Verlag; 2002. p. 91–98.

[15] Krieger A, Susil RC, Fichtinger G, *et al*. Design of a novel MRI compatible manipulator for image guided prostate intervention. *IEEE Trans Biomed Eng* 2005;52:306–313.

[16] Wei Z, Wan G, Gardi L, *et al*. Robot-assisted 3D-TRUS guided prostate brachytherapy: System integration and validation. *Med Phys* 2004;31:539–548.

[17] Stoianovici D, Cadeddu JA, Demaree RD, *et al*. *An efficient needle injection technique and radiological guidance method for percutaneous procedures*. In: *Lecture Notes in Computer Science*, Vol. 1205. Springer Verlag; 1997. p. 295–298.

[18] Stoianovici D, Whitcomb LL, Anderson JH, *et al*. A modular surgical robotic system for image-guided percutaneous procedures. In: *Proceedings to International Conference on Medical Image Computing and Computer-Assisted Intervention*. *Lecture Notes in Computer Science*, Vol. 1496. Springer Verlag; 1998. p. 404–410.

[19] Patriciu A, Stoianovici D, Whitcomb LL, *et al*. Motion-based robotic instrument targeting under C-arm fluoroscope. In: *Proceedings to Medical Image Computing and Computer-Assisted Intervention 2000*. *Lecture Notes in Computer Science*, Vol. 1935. Springer Verlag; 2000. p. 988–998.

[20] Patriciu A, Solomon SB, Kavoussi LR, *et al*. Robotic kidney and spine percutaneous procedures using a new laser-based CT registration method. In: *Proceedings to International Conference on Medical Image Computing and Computer-Assisted Intervention 2001*. *Lecture Notes in Computer Science*, Vol. 2208. Springer-Verlag; 2001. p. 249–257.

[21] Solomon SB, Patriciu A, Bohlman ME, *et al*. Robotically driven interventions: A method of using CT fluoroscopy without radiation exposure to the physician. *Radiology* 2002;225:277–282.

[22] Fichtinger G, DeWeese TL, Patriciu A, *et al*. System for robotically assisted prostate biopsy and therapy with intraoperative ct guidance. *Acad Radiol* 2002;9:60–74.

[23] Stoianovici D, Kavoussi LR, Whitcomb LL, *et al*. Friction transmission with axial loading and a radiolucent surgical needle drive. Provisional U.S. Patent of Invention No. 60/038, 115.

[24] Stoianovici D, Cleary K, Patriciu A, *et al*. AcuBot: A robot for radiological percutaneous interventions. *IEEE Trans Rob Autom* 2003;19:927–930.

[25] Iordachita I, Wiard R, Fichtinger G, *et al*. Controllable motorized devices for accurate percutaneous needle placement in soft tissue target. Proceedings of the 11th World Congress in Mechanisms and Machine Science; 2004. p. 82–86.

[26] Wan G, Wei Z, Gardi L, *et al*. Brachytherapy needle deflection evaluation and correction. *Med Phys* 2005;32:902–909.

[27] Mercier L, Lango T, Lindseth F, *et al*. A review of calibration techniques for freehand 3-D ultrasound systems. *Ultrasound Med Biol* 2005;31:449–471.

[28] Taschereau R, Pouliot J, Roy J, Tremblay D. Seed misplacement and stabilizing needles in transperineal permanent prostate implants. *Radiother Oncol* 2000;55:59–63.

[29] Eapen L, Kayser C, Deshaies Y, *et al*. Correlating the degree of needle trauma during prostate brachytherapy and the development of acute urinary toxicity. *Int J Radiat Oncol Biol Phys* 2004;59: 1392–1394.

[30] Ebrahimi R, Okazawa S, Rohling R, *et al*. Hand-held steerable needle device. In: *Proceedings to Medical Image Computing and Computer-Assisted Intervention 2003*. *Lecture Notes in Computer Science*, Vol. 2879. Springer-Verlag; 2003. p. 223–230.

[31] Kettenbach J, Kronreif G, Figl M, *et al*. Robot-assisted biopsy using computed tomography-guidance: Initial results from *in vitro* tests. *Invest Radiol* 2005;40:219–228.

[32] Kettenbach J, Kronreif G, Figl M, *et al*. Robot-assisted biopsy using ultrasound guidance: Initial results from *in vitro* tests. *Eur Radiol* 2005;15:765–771.